

# **Label-free discrimination of actin and myosin muscle networks using nonresonant contribution of Multiplex-Coherent anti-Stokes Raman Scattering (M-CARS)**

M. Nafa<sup>1</sup>, T. Mansuryan<sup>1</sup>, V. Couderc<sup>1</sup>, L. Magnol<sup>2</sup>, V. Blanquet<sup>2</sup>, F. Baraige<sup>2</sup>, C. Carrion<sup>3</sup>,  
J.-R. Duclère<sup>4</sup>, C. Lefort<sup>1</sup>

1. Université de Limoges, XLIM, UMR CNRS 7252, Limoges, France

2. Université de Limoges, Epidemiology of chronic diseases in tropical zone EpiMaCT, Inserm U1094, IRD  
U270, INRAE USC1501, Limoges, France

3. Université de Limoges, BISCEm, Microscopy core Facility, Limoges, France

4. Université de Limoges, IRCER, UMR CNRS 7315, Limoges, France

## **Abstract**

We propose an original experimental strategy providing evidence for the first label-free disclosure of muscle actin network based on the nonresonant contribution of a multiplex CARS (M-CARS) microscopy setup. Thin actin filaments are known for being located between thick myosin filaments that can be detected in Second Harmonic Generation (SHG) with our M-CARS setup. The first step of our strategy consists in defining spatial regions where thick myosin filaments or thin actin filaments are expected. Then we present an analysis based on two M-CARS spectra corresponding to these regions, which outcome highlights differences in their relative nonresonant contribution. The final step of the presented strategy is their exploitation on each pixel of the M-CARS hyperspectral image, enabling label-free revelation of thin actin filaments. This qualitative imaging represents a proof of principle for highlighting and discriminating purposes in biological microscopy thanks to a difference in the nonlinear properties of the related proteins. Besides, this peculiar imaging technique results from a competition between several four-wave mixing schemes. This paves the way for considering label-free imaging through a competition involving several light-matter interaction effects, rather than considering several of them singularly.

## Introduction

Observation of biological tissues through light-matter interaction has been a hot research topic for decades. Label-free imaging strategies and diagnostics have continuously evolved technically due to the major challenge of eliminating the need for labeling biological substances, particularly in the case of *in vivo* imaging. The use of ultrafast laser pulses in the near infrared range enables to produce specific imaging methods with excellent signal-to-noise ratio through nonlinear light-matter interaction resulting from the nonlinear electrical susceptibility of the substance probed. Multiphoton processes, such as two-photon fluorescence (TPF) or second harmonic generation (SHG), have demonstrated their ability to reveal several proteins label free. Indeed, in some favorable conditions, proteins can be autofluorescent, like elastine or keratine [1], [2], [3], [4]. SHG is noteworthy, as a second order nonlinear susceptibility interaction ( $\chi^{(2)}$ ), allowing for observation of non-centrosymmetric structures of proteins such as collagen or myosin networks [5], [6].

Yet, on the molecular level, not all existing transitions are active for absorption: some of them are only Raman active [7], [8]. In addition, Coherent anti-Stokes Raman Scattering (CARS) [9] is also of major interest in label-free imaging, as it exploits the third-order nonlinear optical susceptibility  $\chi^{(3)}$ . CARS is a four-wave mixing process consisting, first, of the excitation of a coherence between two ro-vibrational levels of some target molecule, implying two waves: namely pump and Stokes [10]. This occurs when the frequency detuning of these two waves and ro-vibrational levels do match, referred hereafter as Raman Shift. Then, such coherence is read by a probe pulse (third wave), resulting in the generation of an anti-Stokes pulse (fourth wave), the frequency of which is determined by the probe frequency plus the Raman Shift. The superposition of the anti-Stokes signal generated for several Raman Shifts represents the resonant CARS response ( $|\chi^{(3)}_{\text{R}}|$ ), and is specific to given molecular groups contained in the molecule. The spectral resolution of the anti-Stokes signal is limited either by the spectral resolution of the probe, or by the apparatus function of the spectrometer used. The studied spectral span corresponds to the maximal frequency detuning achievable between the pump and Stokes pulses [11]. In our group we have an experimental setup, described later, named Multiplex CARS (M-CARS), consisting of using narrowband pump and probe pulses, associated with a broadband supercontinuum Stokes pulse [12]. This setup permits not only to have well resolved anti-Stokes spectra over a broad Raman Shift region (500 – 4000  $\text{cm}^{-1}$ ), but also multimodal hyperspectral imaging through SHG.

Yet, not every pump, Stokes, and probe pulse is engaged in the four-wave mixing scheme described earlier: some are involved in other four-wave mixing schemes [7], [13]. It leads to a constant nonresonant background ( $\chi^{(3)}_{\text{NR}}$ ) that interferes with the resonant response and alters the overall collected  $\chi^{(3)}(\omega)$  spectrum [7], [14]. Concretely, it shifts resonant peaks to lower Raman Shifts, and creates a characteristic rounded signal preceded by a minimum on higher Raman Shifts [14]. The alteration of the overall  $\chi^{(3)}(\omega)$  spectrum illustrates then the competition between CARS and these other interactions. Several techniques have been designed to reduce this nonresonant background, by acting on the polarization states of the pump, Stokes and probe beams [10]; by acting on the delay between the creation of the ro-vibrational coherences and its probing [10]. Regarding multiplex CARS microscopy, Mueller et Zumbusch have suggested that the role of the nonresonant background may be beneficial in improving CARS resonant imaging [15].

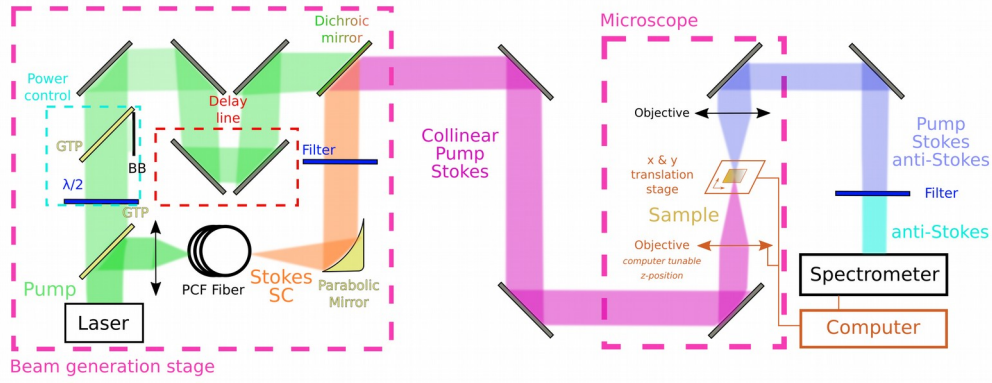
In this publication, we propose investigating the role of the nonresonant background in our M-CARS setup, namely the role of the  $\chi^{(3)}_{\text{NR}} / |\chi^{(3)}_{\text{R}}|$  ratio and its capacity to discriminate features in biomedical imaging that were not originally revealed by label-free techniques. To this end and as an illustration, we have chosen the mouse muscle model with a longitudinally excised Extensor Digitorum Longus (EDL) muscle. The muscle is a biological structure representing 40% of the human body mass. Its ultrafine structure is made of sarcomeres, representing the elementary contractile unit, composed by alternative assembly of thin filaments of actin and thick filaments of myosin [6], [16]. The latter is a noncentrosymmetric structure, which can therefore be characterized with SHG [5], [17]. However, thin filaments of actin are a structure that is possible to image essentially by fluorescence labeling [18], yet cumbersome to image label-free [19]. It is also well known that myosin and actin share very similar CARS spectral signatures [19]. Therefore, we propose to use this biological structure to prove that nonresonant background can be used for highlighting and discriminating purposes in biomedical microscopy. This is based on previous works of the team on inorganic structures imaging. Imaging was possible since, for such structures,  $\chi^{(3)}_{\text{NR}}$  was proportional to the nonlinear refractive index  $n_2$  [20]. Our paper is structured as follows. First, the setup is presented with a focus on the generation of the excitation pulses and the organization of the four-wave mixing approach. Then, we present the revelation of the thick myosin filaments through SHG hyperspectral imaging, enabling to determine two regions: one containing myosin, and an another one containing unrevealed actin networks. Then, typical broadband M-CARS spectra are acquired on the muscle but also on the microscope slide. This trick permits: (1) to isolate an ideal Raman Shift acquisition span, (2) to determine the baseline signal from the

microscope slide to be subtracted and (3) to localize spectrally the resonant and nonresonant contributions to the CARS response. We analyze then M-CARS acquisitions, achieved in our ideal Raman Shift acquisition span, and corresponding to the average of hundreds of spectra assigned to myosin and actin. The differences between the nonresonant and resonant contributions are then exploited on a baseline subtracted M-CARS hyperspectral image, revealing the actin network.

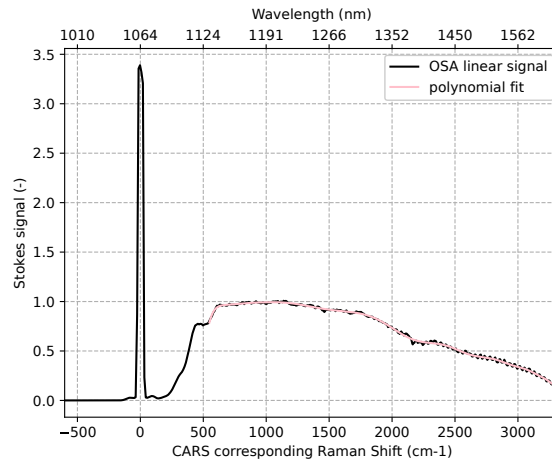
## Experimental setup

The multiplex CARS (M-CARS) experimental scheme is presented in Figure 1 (a). The pump pulse used for our experiment is generated by Q-switched microchip laser source (Horus Laser, 1064 nm, 1 ns, 20 kHz). Part of the pump beam is initially used to generate throughout a PCF fiber a supercontinuum signal, later used as Stokes signal. Its spectrum is represented in Figure 1 (b) and is accompanied by its polynomial fit in the [520, 3300]  $\text{cm}^{-1}$  Raman Shift range, corresponding to the spectral distribution of the M-CARS excitation. In our experiment, the excited coherences are read by the probe beam, which also corresponds to the pump beam. Indeed, part of the nanosecond pulse serves in the creation of the ro-vibrational coherence, part of it to its reading.

Both Stokes and pump are respectively polarized randomly and linearly, so as to take into account every possible light-matter interaction. Once generated and spectrally filtered, the Stokes and pump beams are gathered in a collinear configuration by means of a dichroic mirror (Semrock, NFD01-1064-25x36), and are focused at the sample by a microscope objective (Obj 1: Olympus, UPlanSApo 60x, N.A. = 1.2, water immersion). The anti-Stokes signal is then generated and amplified among this interaction volume, and propagates collinearly with the other beams. In order to detect a collimated anti-Stokes signal, a second microscope objective (Obj 2: Nikon, S Plan Fluor ELWD 60x, N.A. = 0.7) is positioned to collimate the transmitted signal. A filter (Thorlabs, NF1064-44) is placed to filter out any non anti-Stokes contribution before the detection system composed by the spectrometer (Horiba LabRAM HR Evolution, 600  $\text{gr}/\text{mm}$ ) and the CCD camera (Synapse CCD camera, actual spectral resolution  $< 0.8 \text{ cm}^{-1}$ ).



(a)



(b)

Figure 1: M-CARS experimental setup scheme, from beam generation stage to anti-Stokes detection, through CARS interaction at the sample.  $\lambda/2$ , half-wave plate; GTP, Glan-Taylor polarizer; PCF, photonic crystal fiber; BB, beam blocker; SC, supercontinuum. (b) Spectrum of the Stokes supercontinuum pulse (black). The abscissa has been adapted in corresponding CARS Raman Shift scale, taking as reference our narrow pump pulse at 1064 nm. A polynomial fit has been performed on the operating range of the M-CARS setup and is represented in pink.

In the longitudinal axis, the muscle ultrafine structure is constituted by the alternating between actin and myosin filaments. Myosin and actin structures share similar CARS spectra signatures at first sight [19]. For the illustrative application of our strategy, a longitudinally excised EDL muscle is used with a thickness of 4  $\mu\text{m}$ . This sample is placed on a microscope slide (model Superfrost). The

optical focus is first realized in bright-field conditions near the edge of the muscle, leading to the muscle image shown in Figure 2 (a). We remind that our strategy consists first in identifying where the myosin structures are, due to their high response in SHG. Secondly, typical M-CARS spectra are acquired on the muscle but also on the microscope slide to define a baseline signal. M-CARS hyperspectral imaging results are then presented.

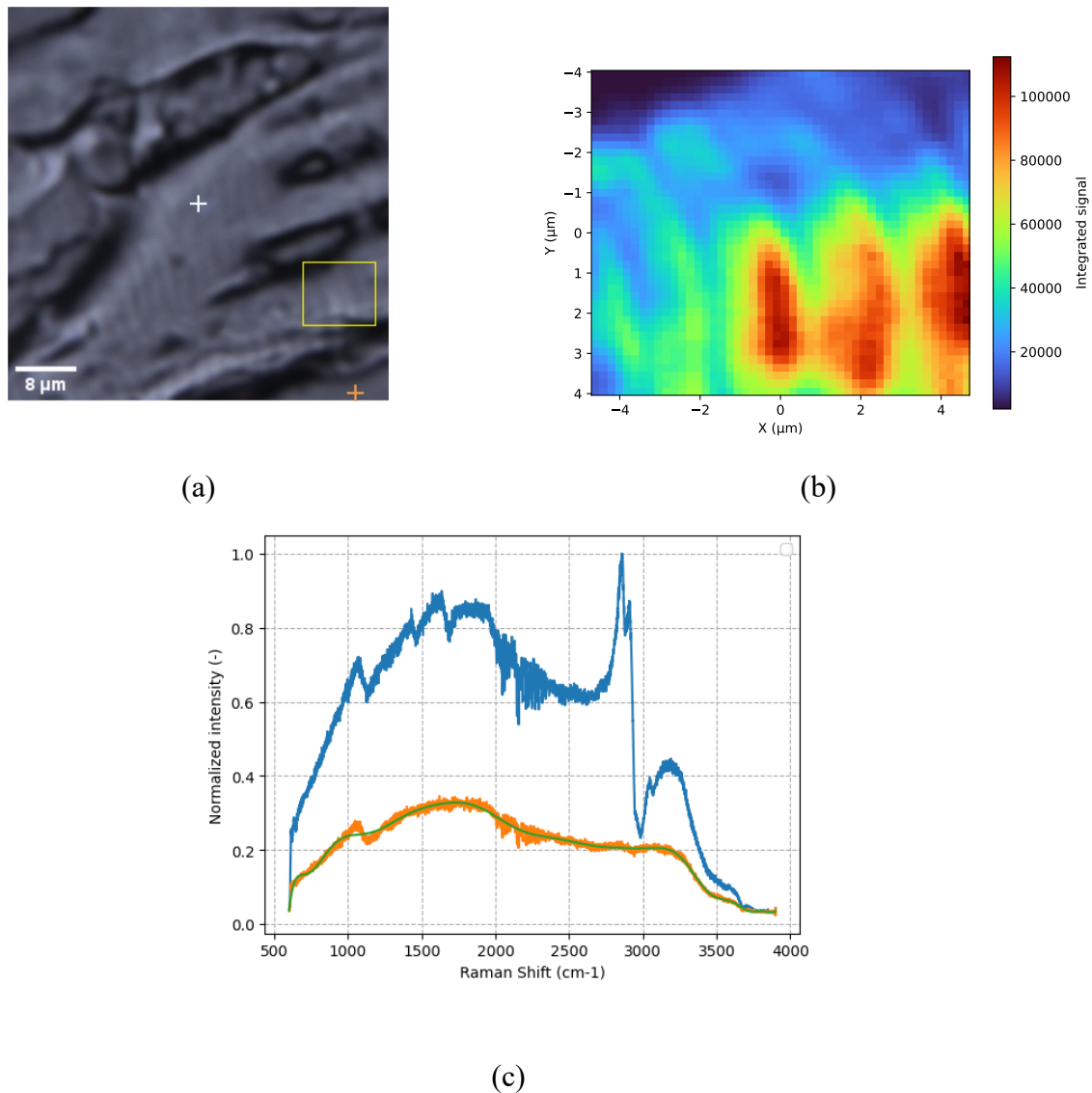


Figure 2: Imaging from the muscle sample: (a) Bright-Field illumination; (b) Second Harmonic Generation ( $t_{exp} = 0.1\text{s}$  per pixel) in the area indicated by the yellow box in (a). (c) Broadband acquisition of CARS spectra at the white and orange markers spotted in (a), respectively plotted in blue and orange. The latter being considered as the response of the Superfrost microscope slide, its polynomial fit is also drawn in green.

## Results and discussion

### Identification of myosin structure through SHG imaging

The first step consists in optimizing the SHG collected signal. We scan the sample inside the yellow box of Figure 2 (a). The detection wavelength range is centered at 532 nm for the detection of the emission of SHG from myosin, leading to the SHG hyperspectral imaging shown in Figure 2 (b). The SHG signal reveals the presence of myosin filaments which can be identified by its dark central stripe. Moreover, thick myosin filaments are spaced by around 2  $\mu\text{m}$ , which corresponds to the usual spacing between them [6], [16].

### Identification of resonant and nonresonant M-CARS contributions

The second step of our strategy consists of considering the M-CARS response that is obtained in the muscle, and on the microscope slide only. Two colored crosses, illustrated in Figure 2 (a), are localizing the corresponding recordings. For each of them, a broadband M-CARS spectrum is acquired over a 1s exposure time. They are presented in Figure 2 (c). The orange spectrum, acquired outside the muscle, reveals the M-CARS signal of the microscope slide alone. The usefulness of this spectrum is to establish a reference baseline, fitted through a polynomial function represented in green, compared to which the M-CARS spectrum of the muscle can be fully interpreted. Indeed, other original features can be observed in the blue spectrum, acquired inside the muscle. A resonant CARS response around 2900  $\text{cm}^{-1}$  can be observed - corresponding to the -CH<sub>2</sub> and -CH<sub>3</sub> stretching groups [3], [21], where the resonant contribution  $|\chi^{(3)}_{\text{R}}|$  is predominant in the  $\chi^{(3)}(\omega)$  response. We can also see around 3000  $\text{cm}^{-1}$  a minimum in intensity followed by a rounded signal. This rounded signal corresponds to the symmetric vibration feature of -OH [21], but is also due to the interference of CARS signal with a nonresonant background ( $\chi^{(3)}_{\text{NR}}$ ). Therefore, we identify the [2600, 3300]  $\text{cm}^{-1}$  Raman shift span as our region of interest, containing not only the  $|\chi^{(3)}_{\text{R}}|$  information (between 2820 and 2920  $\text{cm}^{-1}$ ) but also the  $\chi^{(3)}_{\text{NR}}$  information (further from resonance, for example in the 2600-2650  $\text{cm}^{-1}$  or in the 3150-3250  $\text{cm}^{-1}$  range). Concerning the glass baseline subtraction, we proceed as follows. For each pixel of the M-CARS hyperspectral mapping, the polynomial fit of Figure 2 (c) is normalized and subtracted so that the dip value around 3000  $\text{cm}^{-1}$  reaches a close to zero value. Average behavior of M-CARS spectra in regions assigned to thick

myosin filaments and thin actin filaments is presented in the next section, followed by a discussed presentation of M-CARS imaging results.

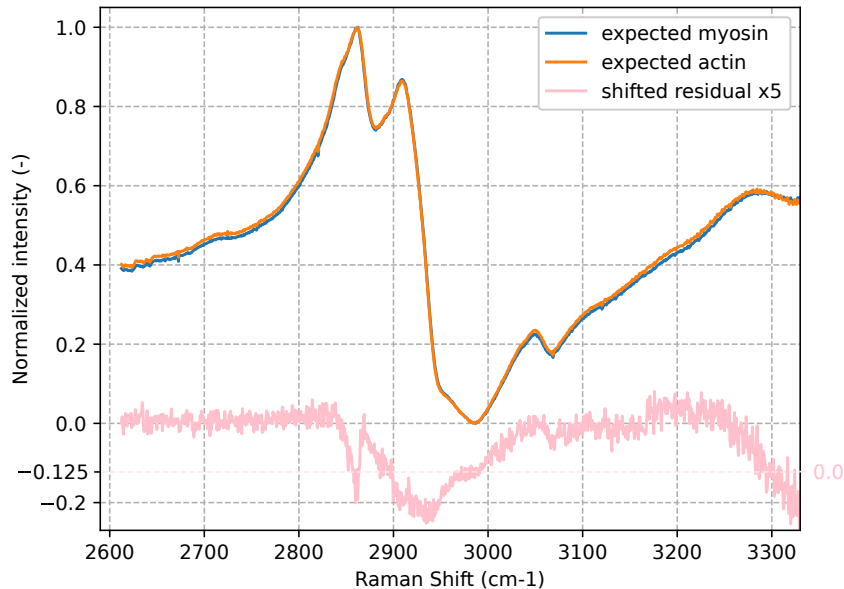


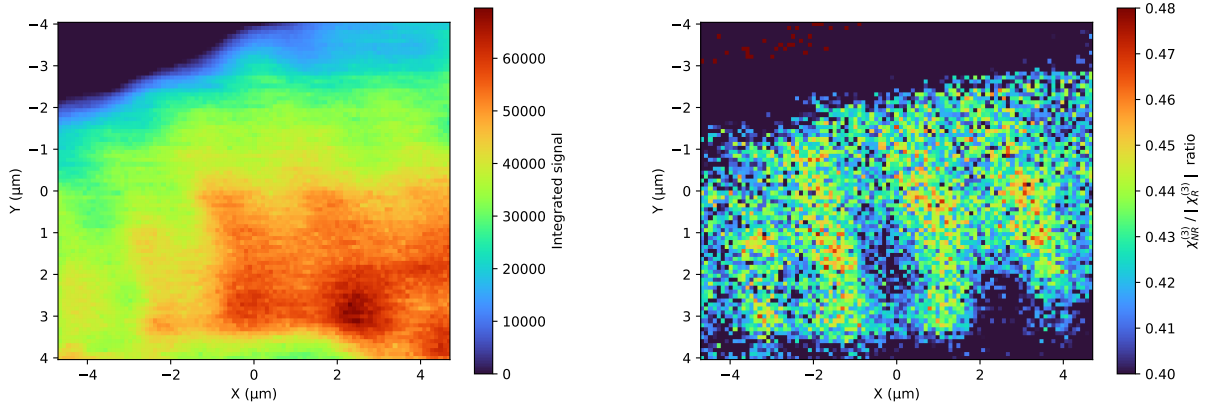
*Figure 3: Average M-CARS spectra from locations highlighted as myosin (blue) or actin (orange) from the SHG image in Figure 2 (b). For sake of clarity, their differences are presented shifted by -0.025, and multiplied by 5 (pink).*

## M-CARS hyperspectral imaging results

M-CARS hyperspectral image has been recorded by mapping the same region of the muscle as for SHG (yellow box in Figure 2 (b)), where glass baseline signal is subtracted as previously explained. Localization of thin actin filaments can be presupposed, since they are known to be contained between myosin structures identified with SHG. Two groups of M-CARS spectra are specifically considered on the basis of their location. Then, for each group, we processed the mean M-CARS spectrum (respectively 1440 and 2430 spectra for actin and myosin were considered) presented them in Figure 3, normalized by the Stokes energy profile distribution of Figure 1 (b). The robustness of the baseline subtraction can be appreciated since the minimum signal always stands near zero. We recall that displaying normalized spectra means that the value assigned to each Raman Shift corresponds to its ratio to the maximal value. Here, the M-CARS resonant signal is

considered with the -CH<sub>2</sub> and -CH<sub>3</sub> stretching contribution ( $|\chi^{(3)}_{\text{R}}|$ ), i.e. between 2820 and 2920 cm<sup>-1</sup>. On this range, the difference between actin and myosin regions are weak, and this observation is reinforced by observing the according resonant M-CARS hyperspectral imaging shown in Figure 4 (a). Thick filaments of myosin can be predicted, yet their contrast with neighboring areas appears to be blurry due to the small difference between actin and myosin regions. No clear information on actin structure can be detected there. However, valuable information can still be extracted from this hyperspectral datacube, when considering the difference between actin and myosin signals further from resonance in Figure 3, where the nonresonant contribution ( $\chi^{(3)}_{\text{NR}}$ ) is predominant. Indeed, the residual signal is there almost constant, around 0.025. Thus, we ultimately consider that the values on these Raman Shifts can be used to evaluate the  $\chi^{(3)}_{\text{NR}}/|\chi^{(3)}_{\text{R}}|$  ratio, and can consequently be used to estimate the relative nonlinear properties for these biological structures, as had been done for inorganic structures [20]. For each M-CARS spectrum of the hyperspectral dataset, the maximal value has been assigned to the CARS resonant contribution  $|\chi^{(3)}_{\text{R}}|$  between 2820 and 2920 cm<sup>-1</sup>, and the  $\chi^{(3)}_{\text{NR}}$  value has been estimated as the mean value between 2600 and 2650 cm<sup>-1</sup>. The corresponding  $\chi^{(3)}_{\text{NR}}/|\chi^{(3)}_{\text{R}}|$  image is presented in Figure 4 (b). It is noticeable that the highlighted features now correspond to what lies between the thick filaments of myosin. This is confirmed by its trimmed superposition made with the SHG image in Figure 5 (a). The 1D plot performed on the latter, shown in Figure 5 (b), shows that the maxima of the myosin image correspond to the minima of the other image and *vice versa* as expected in muscle. Therefore, we claim that this signal represents the thin actin filaments present between the thick filaments of myosin. This result is remarkable because actin can be specifically seen with a correct signal-to-noise ratio, without any addition of fluorophore.

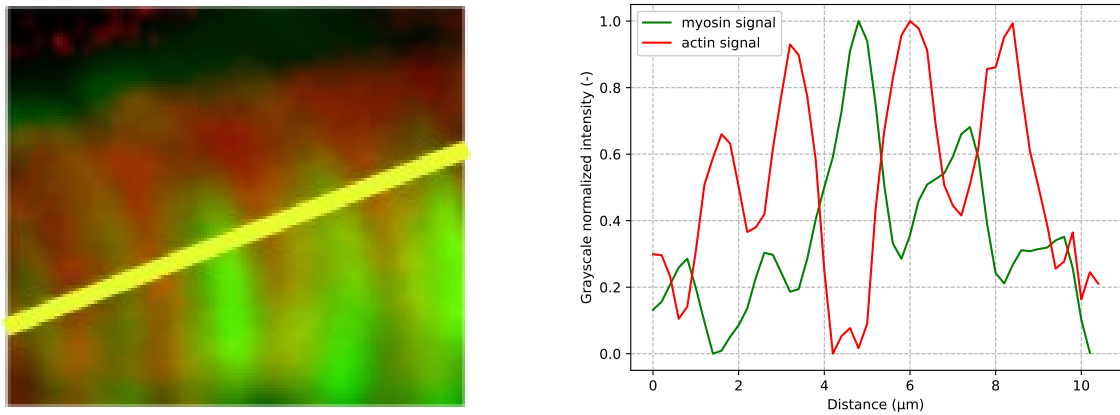
Also, how this image has been obtained, due to the  $\chi^{(3)}_{\text{NR}}/|\chi^{(3)}_{\text{R}}|$  ratio, is remarkable for several reasons. The first, obvious, is practical: performing a ratio is a simple task that is compatible with real-time observations. The second is that the relative nonlinear differences between actin and myosin structures are at the origin of such discrimination. The third reason, is that we considered on the same spectrum, by exploiting nonresonant background, the competition between several four-wave mixing processes, instead of usually considering several light-matter interaction processes singularly in multimodal imaging. One also has to consider that a broadband excitation and a sufficient spectral resolution for the probe pulse are necessary to be able to consider not only resonant CARS features, but also Raman Shifts far away enough that only carries nonresonant CARS contribution.



(a)

(b)

Figure 4: M-CARS hyperspectral imaging: (a) resonant integration between 2820 and 2920  $\text{cm}^{-1}$  ; (b)  $\chi^{(3)}_{NR} / |\chi^{(3)}_R|$  ratio exploiting the interaction between resonant and nonresonant background, the latter being considered as the mean value between 2600 and 2650  $\text{cm}^{-1}$ .



(a)

(b)

Figure 5: (a) Grayscale superposition of the  $\chi^{(3)}_{NR} / |\chi^{(3)}_R|$  ratio image (red, Figure 4 (c)) with the SHG image highlighting thick myosin filaments (green, Figure 2 (b)). The yellow line indicates the direction of the (b) plotted 1D-cropped signals.

## Conclusion

In this paper, a M-CARS setup utilizes a supercontinuum Stokes pulse generated from a narrowband pump pulse to enable multimodal hyperspectral imaging. SHG imaging identifies myosin thick filaments, while a peculiar M-CARS imaging technique, based on the  $\chi^{(3)}_{\text{NR}}/|\chi^{(3)}_{\text{R}}|$  ratio, enables label-free imaging of actin thin filaments with a satisfactory signal-to-noise ratio. This qualitative imaging is a proof-of-principle that nonresonant signal can be helpful to discriminate and identify biological structures, as the team already demonstrated its usefulness for the study of nonlinear properties of inorganic materials. More generally we can state that label-free imaging can not only be considered singularly through one light-matter interaction effect, but rather through the competition involving several of them. Perspectives of this work are multiple. One can be to determine the optimal polarization state for the supercontinuum Stokes pulse so that nonresonant interaction is enhanced. Another one would be a further analysis of the CARS hyperspectral datacubes, through separation of resonant and nonresonant contributions using, for example Maximum Entropy Methods (MEM), Kramers-Krönig transformations, or even deep neural networks [22]. Finally, this technique could be explored to discriminate other biological substances of interest.

## Bibliography

- [1] A.-M. Pena, M. Strupler, T. Boulesteix, et M.-C. Schanne-Klein, « Spectroscopic analysis of keratin endogenous signal for skin multiphoton microscopy », *Opt Express*, vol. 13, n° 16, p. 6268-6274, août 2005, doi: 10.1364/OPEX.13.006268.
- [2] C. Stringari *et al.*, « Multicolor two-photon imaging of endogenous fluorophores in living tissues by wavelength mixing », *Sci. Rep.*, vol. 7, n° 1, p. 3792, juin 2017, doi: 10.1038/s41598-017-03359-8.
- [3] T. Guerenne-Del Ben *et al.*, « Multiplex coherent anti-Stokes Raman scattering highlights state of chromatin condensation in CH region », *Sci. Rep.*, vol. 9, n° 1, p. 13862, sept. 2019, doi: 10.1038/s41598-019-50453-0.
- [4] A. Aghigh, S. Bancelin, M. Rivard, M. Pinsard, H. Ibrahim, et F. Légaré, « Second harmonic generation microscopy: a powerful tool for bio-imaging », *Biophys. Rev.*, vol. 15, n° 1, p. 43-70, févr. 2023, doi: 10.1007/s12551-022-01041-6.
- [5] W. Mohler, A. C. Millard, et P. J. Campagnola, « Second harmonic generation imaging of endogenous structural proteins », *Methods*, vol. 29, p. 97-109, 2003.
- [6] C. Lefort *et al.*, « FAMOUS: a fast instrumental and computational pipeline for multiphoton microscopy applied to 3D imaging of muscle ultrastructure », *J. Phys. Appl. Phys.*, vol. 54, n° 27, p. 274005, juill. 2021, doi: 10.1088/1361-6463/abf8f2.

- [7] S. A. J. Druet et J.-P. E. Taran, « Cars spectroscopy », *Prog. Quantum Electron.*, vol. 7, n° 1, p. 1-72, 1981, doi: [https://doi.org/10.1016/0079-6727\(81\)90002-1](https://doi.org/10.1016/0079-6727(81)90002-1).
- [8] M. Nafa, « Spectroscopie DRASC en régime hybride fs/ps à haute cadence (kHz) appliquée à la thermométrie des gaz. », PhD Thesis, 2017. [En ligne]. Disponible sur: <http://www.theses.fr/2017UBFCD001/document>
- [9] P. D. Maker et R. W. Terhune, « Study of Optical Effects Due to an Induced Polarization Third Order in the Electric Field Strength », *Phys Rev*, vol. 137, n° 3A, p. A801-A818, févr. 1965, doi: 10.1103/PhysRev.137.A801.
- [10] M. Nafa *et al.*, « Ro-vibrational spectroscopy in hybrid fs/ps-CARS for N<sub>2</sub> thermometry », 2017.
- [11] M. Scherman *et al.*, « Rovibrational hybrid fs/ps CARS using a volume Bragg grating for N<sub>2</sub> thermometry », *Opt. Lett.*, vol. 41, n° 3, p. 488, févr. 2016, doi: 10.1364/OL.41.000488.
- [12] Z. Rajaofara *et al.*, « Mapping the second and third order nonlinear susceptibilities in a thermally poled microimprinted niobium borophosphate glass », *Opt. Mater. Express*, vol. 11, n° 10, p. 3411, oct. 2021, doi: 10.1364/OME.433809.
- [13] S. O. Konorov, M. W. Blades, et R. F. B. Turner, « Non-resonant background suppression by destructive interference in coherent anti-Stokes Raman scattering spectroscopy », *Opt. Express*, vol. 19, n° 27, p. 25925, déc. 2011, doi: 10.1364/OE.19.025925.
- [14] F. El-Diasty, « Coherent anti-Stokes Raman scattering: Spectroscopy and microscopy », *Vib. Spectrosc.*, vol. 55, n° 1, p. 1-37, janv. 2011, doi: 10.1016/j.vibspec.2010.09.008.
- [15] M. Müller et A. Zumbusch, « Coherent anti-Stokes Raman Scattering Microscopy », *ChemPhysChem*, vol. 8, n° 15, p. 2156-2170, 2007, doi: 10.1002/cphc.200700202.
- [16] R. W. Craig et R. Padrón, « Molecular Structure of the Sarcomere ».
- [17] S. V. Plotnikov, A. C. Millard, P. J. Campagnola, et W. A. Mohler, « Characterization of the Myosin-Based Source for Second-Harmonic Generation from Muscle Sarcomeres », *Biophys. J.*, vol. 90, n° 2, p. 693-703, janv. 2006, doi: 10.1529/biophysj.105.071555.
- [18] C. Lefort *et al.*, « Multicolor multiphoton microscopy based on a nanosecond supercontinuum laser source », *J. Biophotonics*, vol. 9, n° 7, p. 709-714, juill. 2016, doi: 10.1002/jbio.201500283.
- [19] H. Kim *et al.*, « Coherent Raman Imaging of Live Muscle Sarcomeres Assisted by SFG Microscopy », *Sci. Rep.*, vol. 7, n° 1, p. 9211, août 2017, doi: 10.1038/s41598-017-09571-w.
- [20] Z. Rajaofara *et al.*, « Measurement of the third order nonlinear susceptibility of paratellurite single crystal using multiplex CARS », *AIP Adv.*, vol. 9, n° 10, p. 105301, oct. 2019, doi: 10.1063/1.5113478.
- [21] A. Silve, N. Dorval, T. Schmid, L. M. Mir, et B. Attal-Tretout, « A wide-field arrangement for single-shot CARS imaging of living cells », *J. Raman Spectrosc.*, vol. 43, n° 5, p. 644-650, mai 2012, doi: 10.1002/jrs.4051.
- [22] R. Junjuri, A. Saghi, L. Lensu, et E. M. Vartiainen, « Effect of non-resonant background on the extraction of Raman signals from CARS spectra using deep neural networks », *RSC Adv.*, vol. 12, n° 44, p. 28755-28766, 2022, doi: 10.1039/D2RA03983D.